

## The magmatic relationship between the “Kurotani ultra-mafic rock” and the Ordovician(?) Iwatsubodani Formation, Takayama City, Hida Gaien belt, central Japan: the chemical composition of clinopyroxene

TSUKADA Kazuhiro<sup>1\*</sup>, SHIMURA Yusuke<sup>2</sup>, and NADMID Bayart<sup>2</sup>

<sup>1</sup> The Nagoya University Museum, Nagoya 464-8601, Japan

<sup>2</sup> Graduate School of Environmental Studies, Nagoya University, Nagoya 464-8601, Japan

\*Corresponding author: Tel.: +81-52-789-5768; Fax: +81-52-789-5896

*E-mail address:* tsukada@num.nagoya-u.ac.jp (K. Tsukada)

### Abstract

A major problem for understanding the tectonic history of the Inner zone of Southwest Japan is the spatial tectonic contrast between the rocks in its western and eastern parts. In the western part of the zone, the Sangun–Renge, Akiyoshi, Maizuru, and Ultra-Tanba belts are widely exposed, whereas they are fragmented in a narrow area along the Hida Gaien belt in the eastern part. The Hida Gaien belt with its fault-bound blocks is thus a key unit for understanding the geology. The lithostratigraphy and structure of the blocks composed of volcanic/sedimentary rocks have been studied previously (e.g., Tsukada et al., 2004), but few attempts have been made to study the blocks of ultra-mafic rock which are critical to understanding the tectonic process in the Hida Gaien belt. In the Nakao area, Takayama City, Ordovician(?) mafic volcanic rocks (the Iwatsubodani Formation) of the Hida Gaien belt have been thrust onto an unclassified block of Kurotani ultra-mafic rock (KUM). This paper describes the mineral chemical composition of rocks from the KUM and the Iwatsubodani Formation and discusses the magmatic relationship between their clinopyroxene (Cpx) chemical composition.

The Mg# (= Mg/(Mg + Fe) mol%) of Cpx in the KUM is 0.93–0.98. In the Iwatsubodani Formation, sub-ophitic lava (Mg# of interstitial Cpx = 0.41–0.79) is overlain by pyroclastic rock with abundant clasts of porphyritic lava (Mg# of Cpx porphyry = 0.75–0.90). In the variation diagram, most elements of Cpx from the KUM and Iwatsubodani Formation form a linear trend against Mg#. Thus, the KUM and Iwatsubodani Formation probably both originated through fractionation from a single magma source. Although the porphyritic lava overlies sub-ophitic lava in the Formation, the Mg# of Cpx in the porphyritic lava is much higher than that of the underlying sub-ophitic lava. This fact suggests that the Cpx porphyry of the porphyritic lava had probably crystallized in a magma chamber before the sub-ophitic lava stage.

**Key words:** ultra-mafic rock, Iwatsubodani Formation, clinopyroxene chemical composition, Hida Gaien belt, central Japan

### Introduction

The Inner zone of Southwest Japan (SW Japan) is divided into eight geological belts: Hida, Hida Gaien, Sangun–Renge (including Oeyama ophiolite and Sangun–Renge metamorphic rocks), Akiyoshi, Maizuru, Ultra-Tanba, Mino–Tanba, and Ryoke belts (e.g., Taira et al., 2016: Fig. 1). In the western part of the Inner zone, the rocks of the Sangun–Renge, Akiyoshi, Maizuru, and Ultra-Tanba belts have been thrust onto those of the Mino–Tanba belt. However, in the eastern part of this zone, the constituents of these belts are fragmented in a narrow area along the Hida Gaien belt (HGB) (e.g., Tsukada et al. 2004; Taira et al., 2016: Fig. 1). The lithostratigraphy and geological structure in and around the HGB is critical to understanding this contrast and in revealing the tectonic

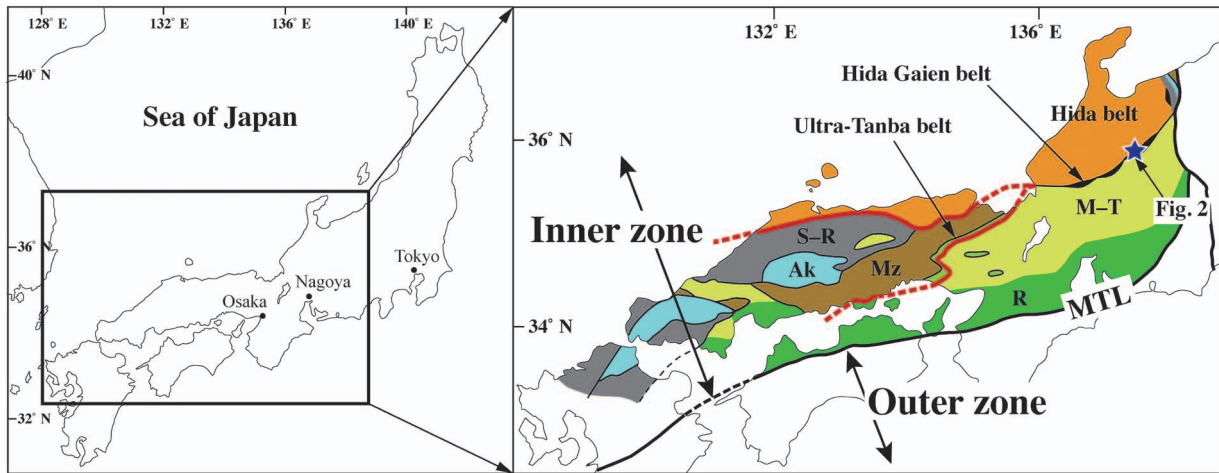


**Fig. 1** Tectonic map of SW Japan (modified from Taira et al., 2016). S-R: Sangun-Renge belt, Ak: Akiyoshi belt, Mz: Maizuru belt, M-T: Mino-Tanba belt, R: Ryoke belt, MTL: Median Tectonic Line.

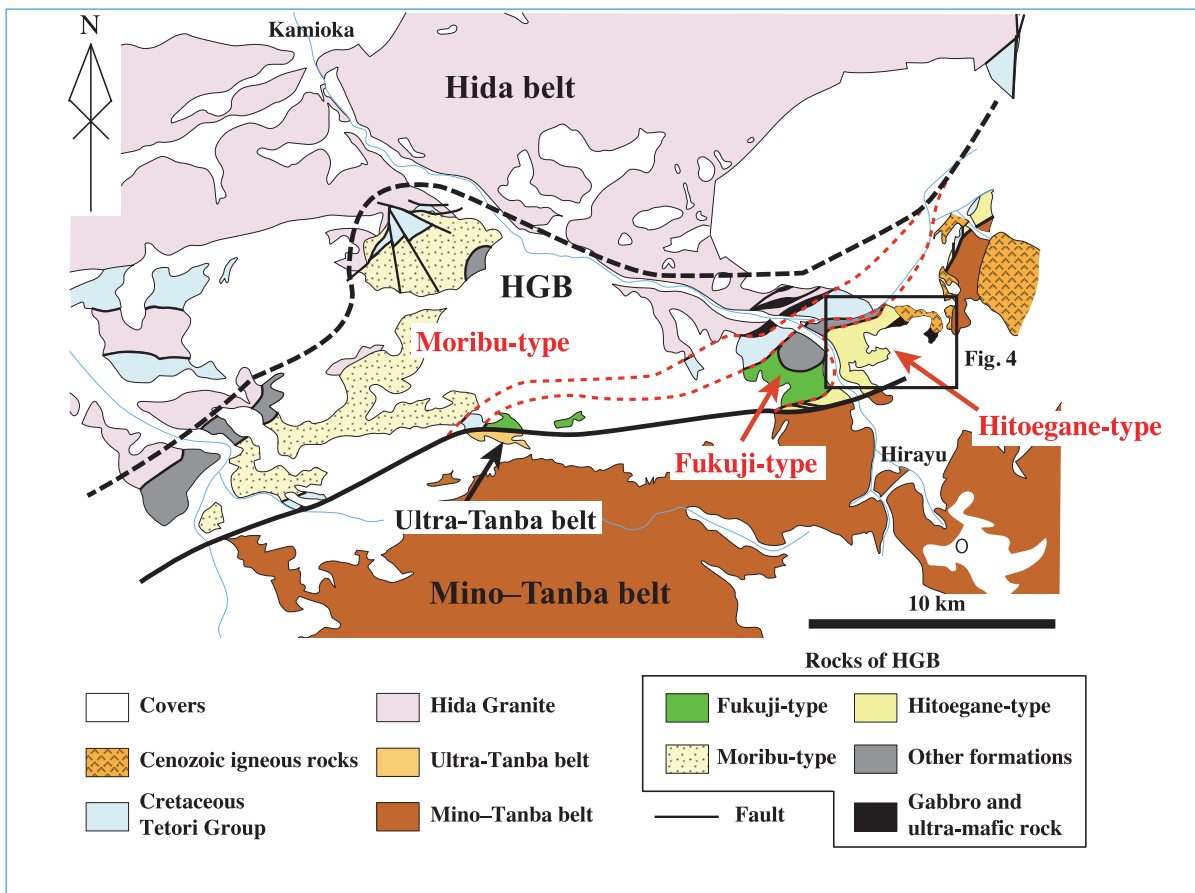


**Fig. 2** Tectonic division of the Hida Gaien belt in the Takayama area, central Japan (modified from Tsukada et al., 2017).

history of SW Japan. Tsukada et al. (2004, 2017) showed that the lithostratigraphy of the HGB includes three types of fault-bound blocks which are divided by brittle/ductile shear zones: Hitoegane, Fukuji, and Moribu (Figs. 2 and 3). However, few attempts have been made to study the age, lithostratigraphy, and geochemistry of other blocks,

in particular the ultra-mafic rocks scattered within the HGB, so the detailed tectonic history of this belt has not yet been clarified.

In the Nakao area, Takayama City, central Japan, Ordovician(?) mafic volcanic rocks (Iwatsubodani Formation) of the Hitoegane-type block have been thrust onto an unclassified Kurotani ultra-mafic rock (KUM) (Figs. 2 and 4). The chemical composition of the minerals is important in considering the magmatic relationship between the KUM and the surrounding volcanic rocks, and helps to elucidate the process of development of the HGB. This paper describes the chemical composition of minerals in the KUM and the Iwatsubodani Formation, and discusses the magmatic relationship between the KUM and the Iwatsubodani Formation, based on the chemical composition of their clinopyroxene (Cpx).

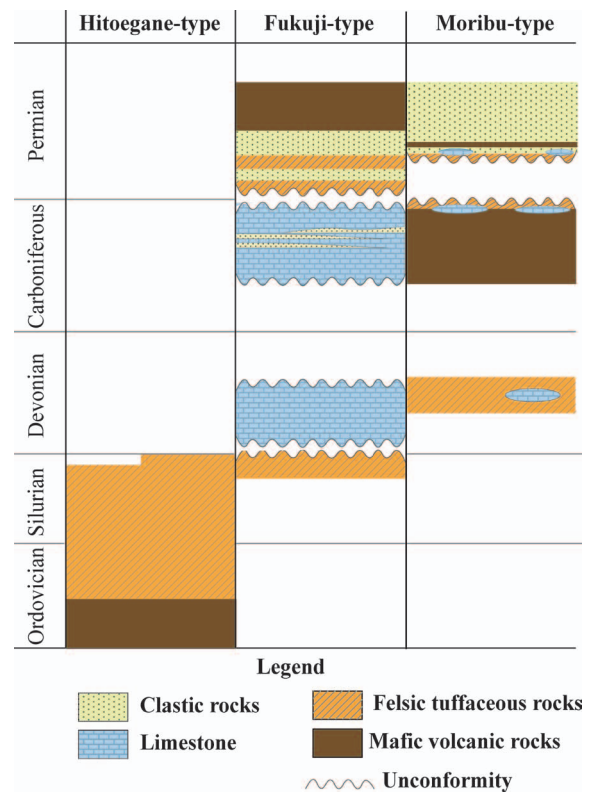


**Fig. 3** Schematic stratigraphies of the Hitoegane, Fukuji, and Moribu-type successions in the Hida Gaien belt (modified from Tsukada, 2003, Ehiro et al., 2016, and Tsukada et al., 2017).

### Definition of the Hida Gaien Belt

A “geological belt” can be defined as an area with common geological characteristics and any geologic divisions must still retain those characteristics. The rocks of the Hida Gaien belt (Kamei, 1955) can be divided into four groups according to their lithology and structure (Fig. 5): (1) Paleozoic–Mesozoic shallow-marine formations; (2) serpentinite mélangé including metamorphic rocks older than 300 Ma (equivalent to the Sangun–Renge belt). (3) Permian accretionary complex (equivalent of the Akiyoshi belt); (4) pre-Permian gabbro and Permian clastic rocks (equivalent to the Maizuru belt) (e.g., Tsukada et al., 2004). These groups are regularly arranged in sequence from the inner (west or north) to the outer (east or south), each with its own distribution area (Fig. 5). For example, (1) is always exposed in the innermost area (west or north) and is never exposed east or south of (2), (3), or (4) (Fig. 5). Each of the four groups therefore has its own characteristic geological features and position and deserves recognition as a separate geological unit. Updating Kamei’s (1955) definition, Tsukada et al. (2004) defined the HGB as a geological unit composed mainly of Paleozoic–Mesozoic shallow-marine formations with their metamorphic facies lying between the Hida metamorphic rocks and the Sangun–Renge belt. This corresponds closely with group (1) of Kamei’s HGB. Subsequently, Kunugiza and Maruyama (2011) updated their definition of the HGB as a “serpentinite mélangé belt,” which includes all the rocks of groups (1) to (3) (Fig. 5).

Since a geological division is a grouping of strata and rock bodies that share common geological characteristics, it is not appropriate to amalgamate groups (1) to (3), because they have different geological features and positions. Besides, it would not be correct to bring these together as a “serpentinite mélangé belt,” because Kunugiza and Maruyama (2011) did not observe serpentinite mélangé structures in most of the HGB. Indeed, serpentinite is

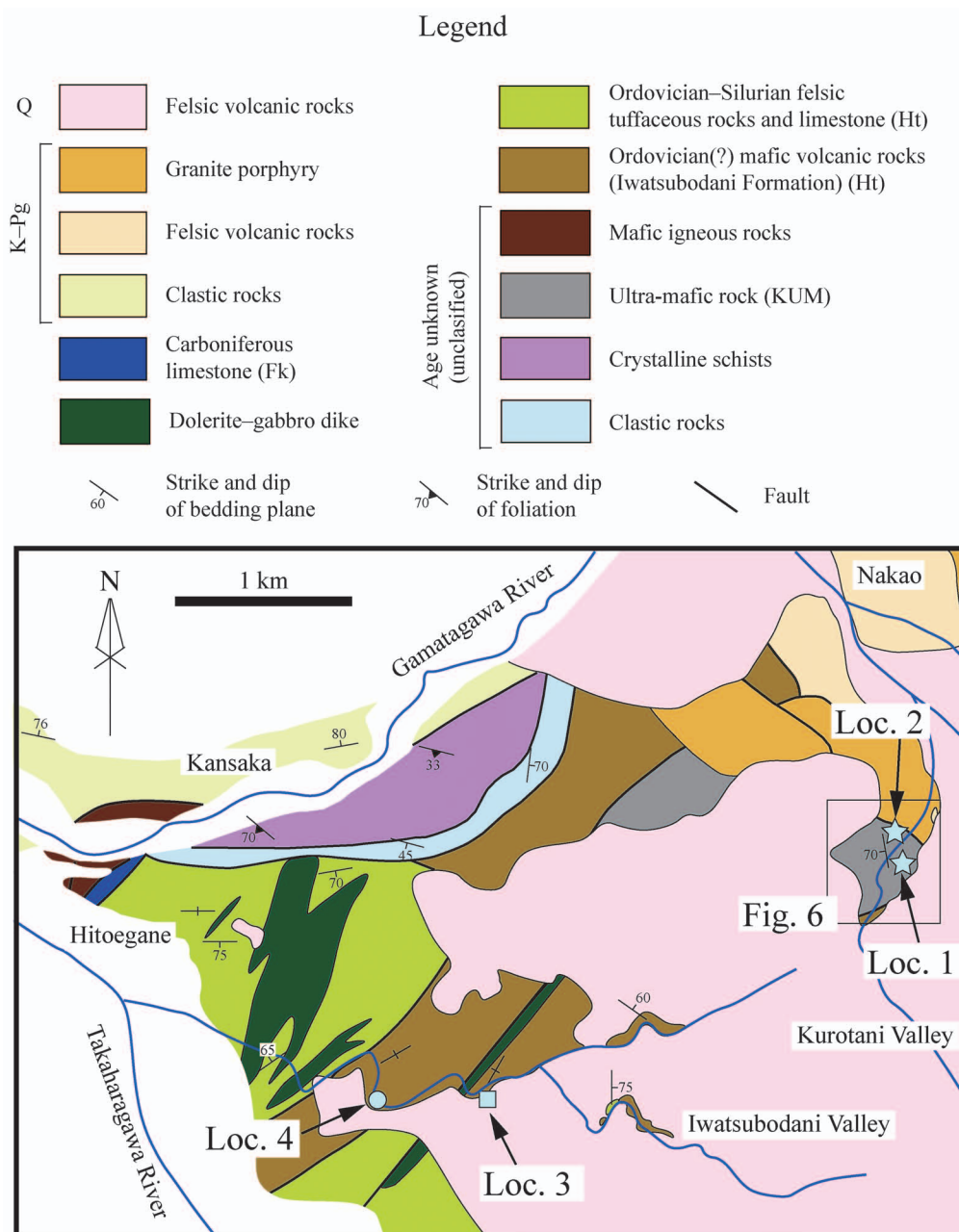


**Fig. 4** Geological map of the Hitoegane–Nakao area. K: Cretaceous, Pg: Paleogene, Q: Quaternary, Ht: Hitoegane-type, Fk: Fukuji-type.

an extremely minor component throughout most of the HGB (Kunugiza and Maruyama, 2011), and Paleozoic–Mesozoic shallow-marine formations are never exposed as a “block” in a serpentinite-matrix (e.g., Tsukada et al., 2004 and references therein: Figs. 3–5). It is true that shallow-marine rocks are isolated within the serpentinite mélangé in one occurrence of group (2), which is the equivalent of the Sangun–Renge belt at the Shiroumadake area (Takeuchi et al., 2004: Fig. 5). But this structure is not a primitive feature of the belt and is likely to be the result of recent tectonic movement (Takeuchi et al., 2004). For these reasons, this paper uses the divisions described by Tsukada et al. (2004).

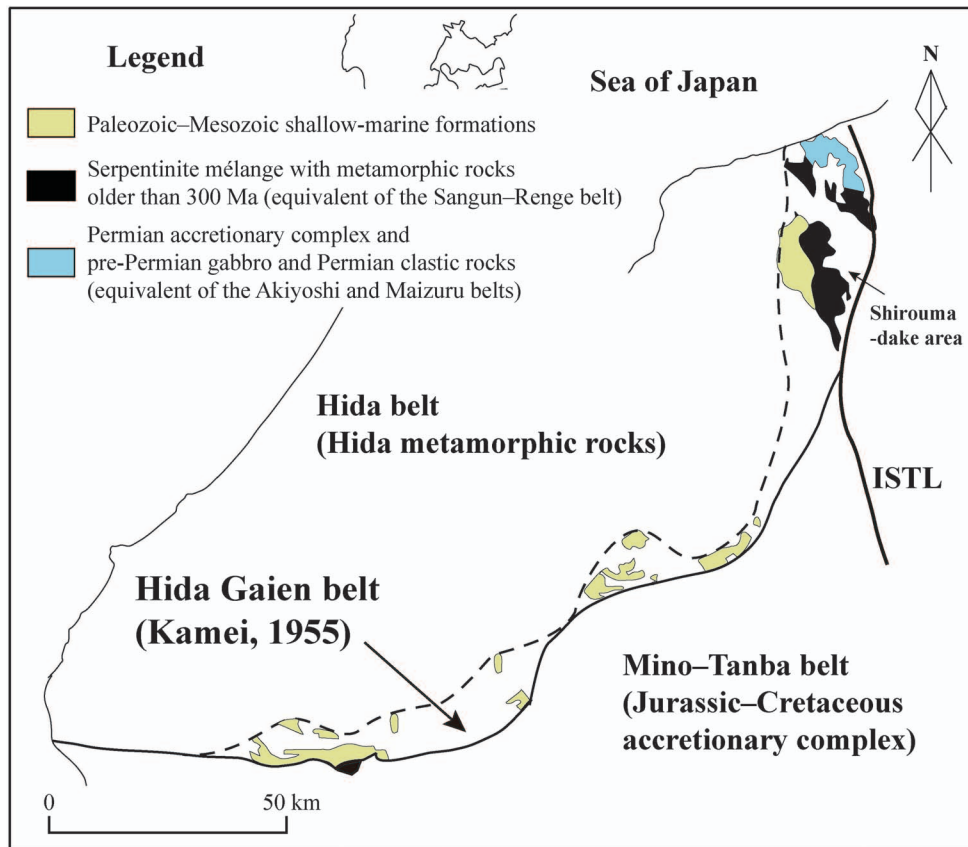


**Fig. 5** Classification of the Hida Gaien belt (Kamei, 1955). ISTL: Itoigawa–Shizuoka Tectonic Line.

### Geological framework of the Hida Gaien Belt

The Hida Gaien belt includes fault-bound blocks of Paleozoic–Mesozoic rocks which can be divided into the following three types based on their lithostratigraphy: (1) Hitoegane-type composed of Ordovician(?) mafic volcanic rocks, Ordovician to Silurian felsic tuffaceous rocks, and clastic rocks; (2) Fukuji-type composed mainly of Silurian felsic tuffaceous rocks and clastic rocks, Devonian limestone, Carboniferous limestone, and Permian felsic tuffaceous rocks, clastic rocks, and mafic volcanic rocks; and (3) Moribu-type composed of Devonian felsic tuffaceous rocks, Carboniferous mafic pyroclastic rocks, and Permian clastic rocks (Ehiro et al., 2016; Tsukada et al., 2004: Figs. 2–4).

In the Hitoegane-type, the mafic volcanic rocks, which are named Iwatsubodani Formation (Tsukada, 1997), are in fault contact with Ordovician–Silurian felsic tuffaceous rocks. However, the evidence is that the former was originally overlain by the latter (Tsukada, 1997; Tsukada et al., 2017) and if so, the Iwatsubodani Formation is older than Silurian, probably of Ordovician age. The upper part of the Ordovician–Silurian tuffaceous rocks corresponds to a part of the Fukuji-type (Kamei, 1955; Manchuk et al., 2013; Ehiro et al., 2016: Figs. 3 and 4).

In the Fukuji-type, the Silurian tuffaceous rocks, Middle Devonian limestone, Carboniferous limestone, and Lower to Middle Permian felsic tuffaceous rocks and clastic rocks are in fault contact with each other, but they are likely to have formed a superposing succession (e.g., Igo, 1956; Niikawa, 1980; Adachi, 1985; Igo, 1990; Tsukada and Takahashi, 2000: Fig. 3). The Permian felsic tuffaceous rocks and clastic rocks are conformably overlain by Middle Permian mafic volcanic rocks (Tsukada et al., 1999; Tsukada and Takahashi, 2000: Fig. 3).

In the Moribu-type, the Devonian formation is in fault contact with other Paleozoic formations (Tazawa et al.

1997, 2000b). The Carboniferous mafic–felsic volcanic rocks are unconformably overlain by Middle Permian clastic rocks (e.g., Horikoshi et al., 1987; Tazawa et al., 1993; Tazawa et al., 2000a; Niwa et al., 2004; Tsukada and Niwa, 2005: Fig. 3).

In addition, unclassified small blocks of ultra-mafic rock including the KUM, mafic volcanic-plutonic rocks, felsic volcanic rocks, and clastic rocks are enclosed in the HGB (Figs. 2 and 4).

### Geological description of the Kurotani Ultra-Mafic rock and the Iwatsubodani Formation

#### *Kurotani ultra-mafic rock (KUM)*

The KUM, exposed at the Kurotani Valley, Nakao area, Takayama City, has been thrust onto Paleogene granite porphyry (Harayama, 1990) with a brittle shear zone (Figs. 4, 6, and 7a, b). The shear zone is composed of loose gouge and foliated cataclasite which strikes N 40° W and dips 50° to the south. Mafic volcanic rock of the Iwatsubodani Formation has been thrust over the KUM with a consolidated brittle-ductile shear zone trending northeast and moderately dipping south (Fig. 6). The  $\sigma$ -type asymmetric structure in the shear zone shows a top-to-the-northwest sense of shear (Fig. 7c).

The KUM has been serpentized and subsequently suffered thermal metamorphism to yield tremolite. It includes the following three types of rock according to their mineral assemblage: (1) serpentine + olivine + tremolite + Cr-spinel; (2) serpentine + olivine + Cr-spinel; and (3) serpentine + olivine + tremolite + clinopyroxene (Cpx). Locality 1 has an exposure of rock types (1) and (2), while locality 2 is of rock type (3) (Fig. 6). At locality 1, rock types (1) and (2) form a rhythmic layering suggesting cumulate (Figs. 6 and 7d–f). In addition, slump structure and cross-lamina are recognized there (Fig. 7g, h). The layering strikes north and dips steeply west (Fig. 6).

These rocks are largely composed of bladed/fibrous antigorite and chrysotile, and generally include magnetite, pyrite, ferric-chromite, and talc (Fig. 8a). Serpentine partly shows bladed-mat texture. In places, sheets of granular Fe-oxide minerals form a layering structure (Fig. 8b). Cleavages are generally developed in olivine to form “cleavable olivine” (Kuroda and Shimoda, 1967: Fig. 8c). Olivine is clearly distinguished into two groups in terms of their brightness in back-scatter electron imaging (Fig. 8d). Darker olivine is generally embedded in brighter one, and they gradually merge into each other without distinct boundary (Fig. 8d). Olivine pseudomorphs, represented by an aggregation of granular magnetite and pyrite, are rarely included in the KUM (Fig. 8e). The Cr-spinel is, in most cases, rimmed by, or sporadically included within the magnetite (Fig. 8f). Serpentine, olivine, and Cpx are cut by slender or acicular tremolite to give a decussate texture (Fig. 8g). The Cpx, which is granular, columnar, or wedge-shaped, can on rare occasions be entirely embedded in tremolite (Fig. 8h). Serpentine was produced along cleavages of the Cpx (Fig. 8h).

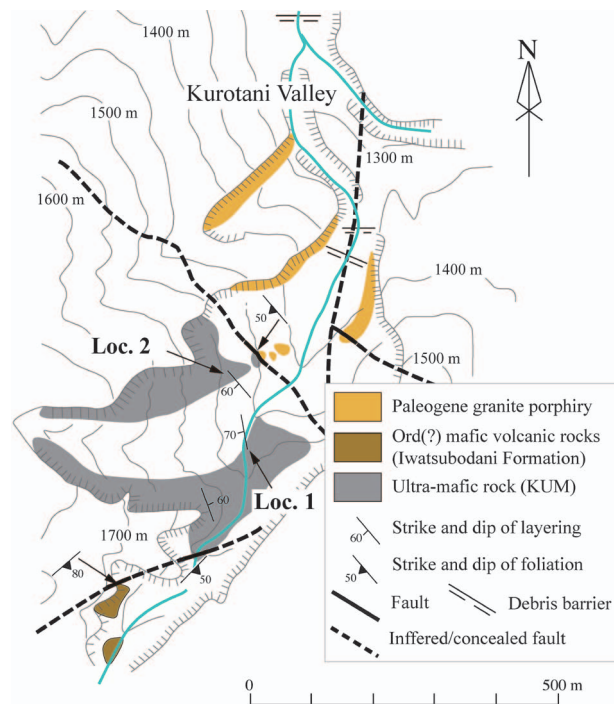


**Fig. 6** Route map along the Kurotani Valley. Ord: Ordovician.

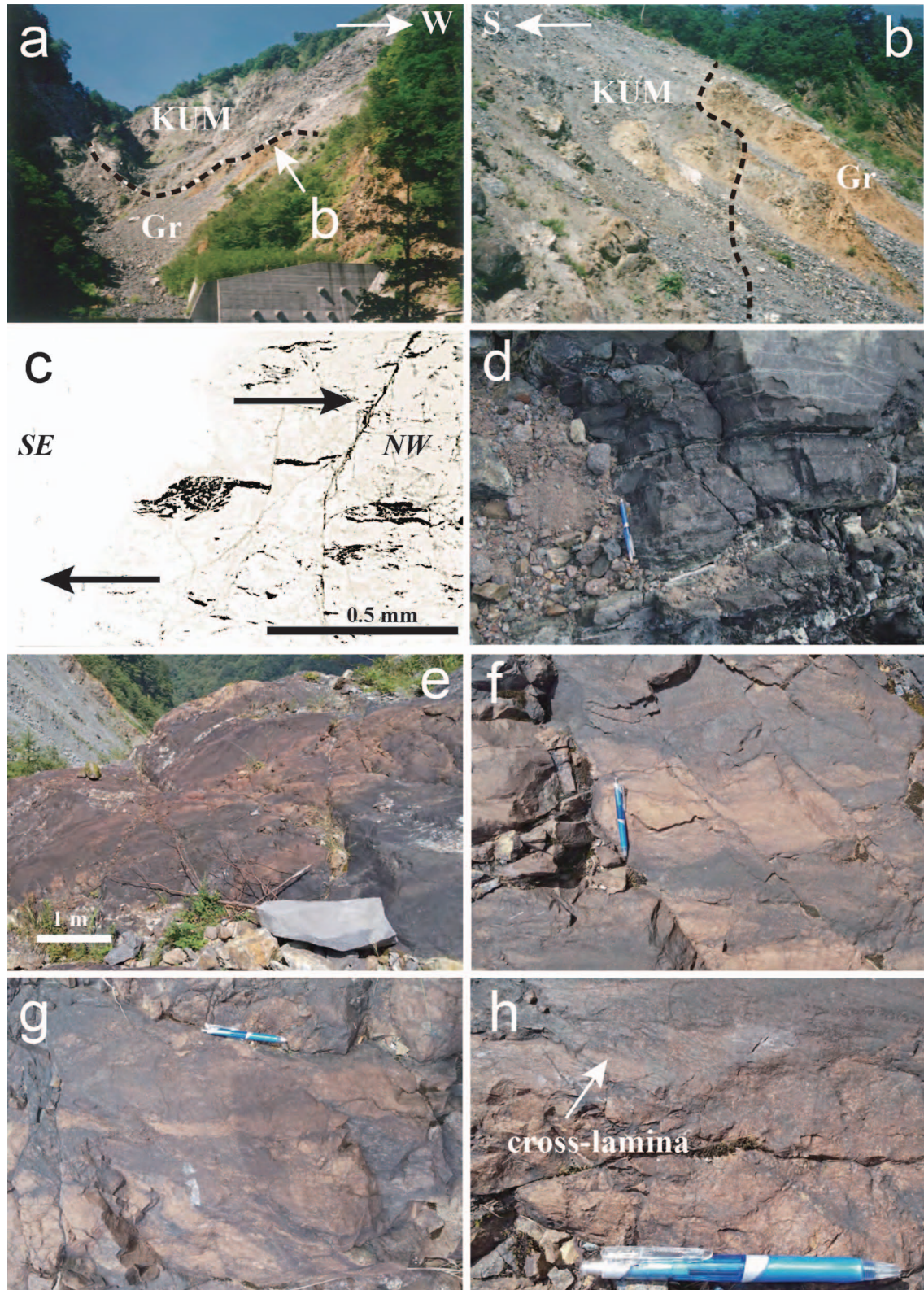


**Fig. 7** Field occurrence of the Kurotani ultra-mafic rock (KUM). (a, b) Relationship between the KUM and the Paleogene granite porphyry (Gr). Broken line shows the boundary between the KUM and the granite porphyry. The KUM has been thrust onto the Paleogene granite porphyry with a brittle shear zone. (c) Photomicrograph of the brittle-ductile shear zone bounding the KUM and the Iwatsubodani Formation. A  $\sigma$ -type asymmetric structure of an iron-oxide mineral shows top-to-the northwest movement. Plane polarized light. (d, e) Layered ultra-mafic rock at locality 1. (f–h) Close-up view of (e). (f) Layered structure by an alternation of white (serpentine + olivine + tremolite + Cr-spinel) and black (serpentine + olivine + Cr-spinel) layers. (g) A slump structure in the KUM. (h) A cross-lamina in the KUM.

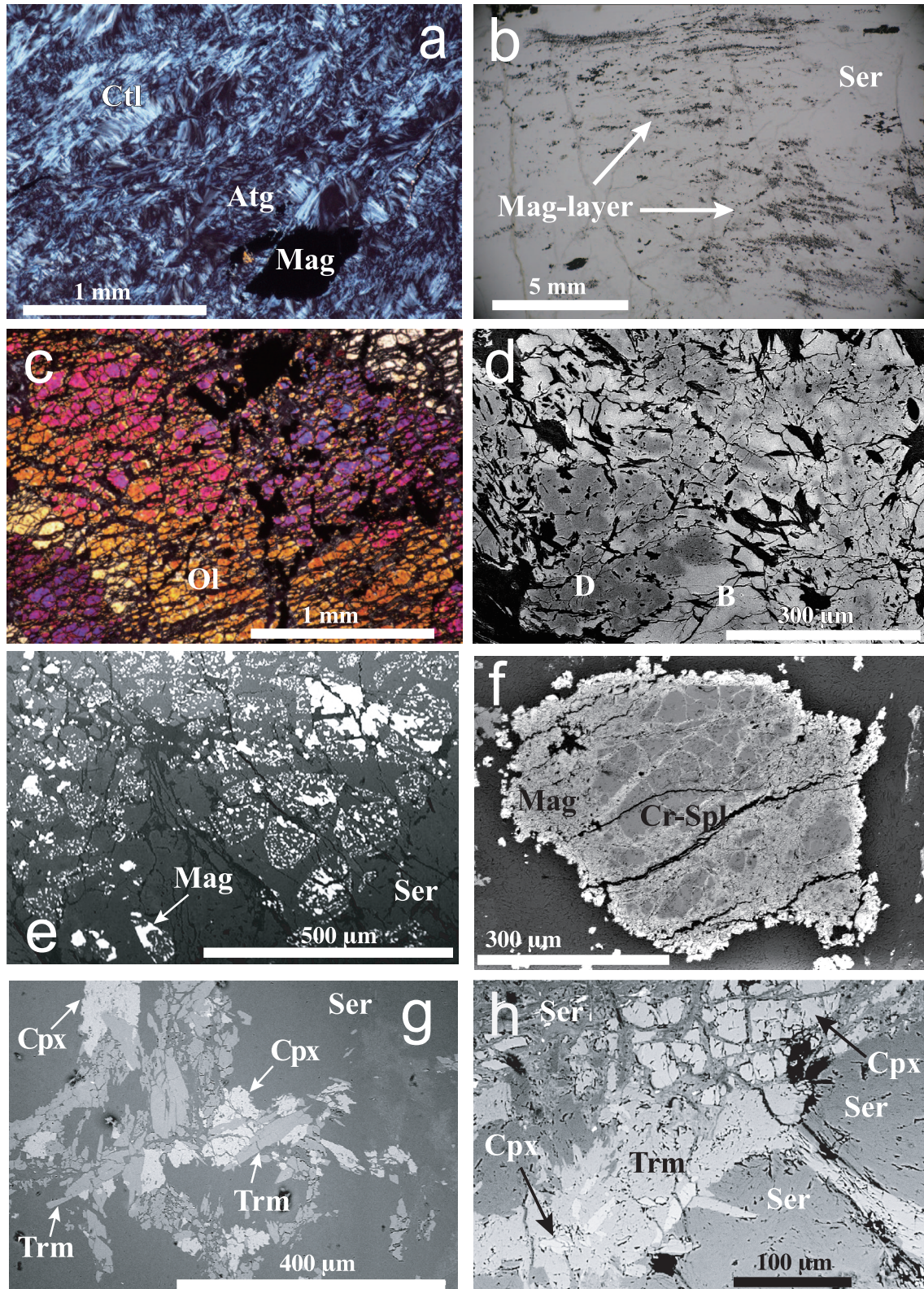


**Fig. 8** Photomicrographs of the ultra-mafic rock of the Kurotani ultra-mafic rock (KUM). (a) Serpentinite in the KUM. (b) Layers by granular magnetite. Plane polarized light. (c) Cleavable olivine. Crossed polar. (d) Back scatter electron image showing two groups olivine. D: darker olivine, B: brighter olivine. (e) Olivine pseudomorphs represented by aggregation of granular magnetite and pyrite. Back scatter electron image. (f) Cr-spinel enclosed by magnetite. Back scatter electron image. (g) Back scatter electron image showing tremolite cutting clinopyroxene. (h) Cleavages of Clinopyroxene are filled by serpentine. Clinopyroxene entirely embedded in tremolite. Back scatter electron image. Atg: Antigorite, Cpx: clinopyroxene, Cr-spl: Cr-spinel, Ctl: Chrysotile, Mag: magnetite, Ol: olivine, Ser: serpentine, t-1: type-1 olivine, t-2: type-2 olivine, Trm: tremolite.

### *Iwatsubodani Formation*

The Iwatsubodani Formation, mainly exposed along the Iwatsubodani valley, Hitoegane area, Takayama City, is composed of mafic lava and pyroclastic rock (Figs. 4 and 9a, b). The lava, overlain by pyroclastic rock, shows eastward-up pillow structure in the upper reach of the valley (Tsukada et al., 2017: Fig. 9a). The lava is generally fine-grained with a sub-ophitic texture, and the majority of the euhedral plagioclase and anhedral Cpx are fresh and clear (Fig. 9c). The lava is partly altered to the extent that some minerals have been replaced by secondary minerals such as chlorite, muscovite and opaque minerals. The pyroclastic rock includes abundant angular clasts of mafic lava, from several millimeters to tens of centimeters in diameter (Tsukada et al., 2017: Fig. 9b). The majority of clasts, which represent the igneous activity of the pyroclastic rock formation, have a porphyritic texture with phenocrysts (Fig. 9d). In addition, clasts showing a sub-ophitic texture similar to the pillow lava described above are rarely included in the pyroclastic rock (Tsukada et al., 2017). Larger phenocrysts of euhedral plagioclase and Cpx are scattered in smaller interstitial patches of plagioclase in the porphyritic clast (Fig. 9d). The plagioclase was generally albitized and replaced by secondary minerals in places. In this paper, lava with a sub-ophitic texture is referred to as basalt A, and clast with a porphyritic texture in the pyroclastic rock as basalt B following Tsukada et al. (2017) (Figs. 4 and 9).

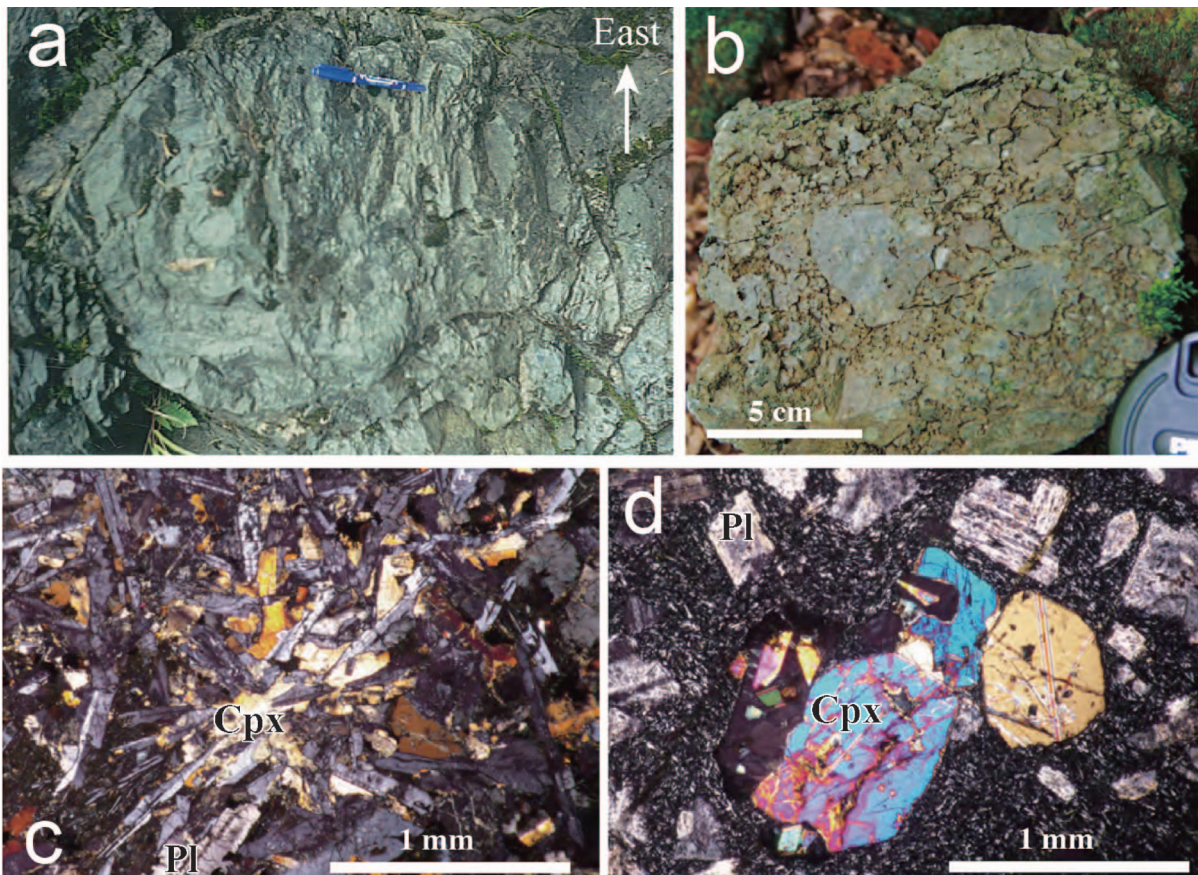


**Fig. 9** (a, b) Field occurrence of the Iwatsubodani Formation. (a) Pillow lava with eastward-up structure having sub-ophitic texture (basalt A). (b) Pyroclastic rock with abundant clasts of porphyritic lava (basalt B). (c, d) Photomicrographs of the mafic lava of the Iwatsubodani Formation. (c) Sub-ophitic texture of the basalt A. (d) Porphyritic texture of the basalt B. Cpx: clinopyroxene, Pl: plagioclase.

## Mineral chemical composition

The chemical composition of the minerals in the KUM and of basalts A and B of the Iwatsubodani Formation were determined by a method described in Tsukada (2018, 2021) using an Energy Dispersive X-ray spectrometer (Oxford X-Max) linked with the Scanning Electron Microscope (Hitachi S-3400N) at Nagoya University Museum. In most cases, the relative error of the analysis was <5% when the measured level was more than 1 wt%, and <10% when the measured level was less than 1 wt% (Tsukada, 2018, 2021). Elements with a concentration of less than 0.5 wt% may not have been detected (Tsukada, 2018, 2021). The representative chemical composition of each of the minerals in the KUM and the mafic lava are shown in Table 1. Molar  $\text{Fe}^{2+}$  and  $\text{Fe}^{3+}$  of Cr-spinel in the KUM were stoichiometrically calculated.

**Table. 1** Representative chemical composition of the clinopyroxene from the Kurotani ultra-mafic rock (KUM) and the basalts A and B of the Iwatsubodani Formation.

	Kurotani ultra-mafic rock						Iwatsubodani Formation	
	Olivine			Clinopyroxene (n = 191)	Tremolite (n = 120)	Cr-spinel (n = 42)	Basalt A	Basalt B
	t-1 (n = 172)	t-2 (n = 216)	t-3 (n = 21)				Cpx (n = 125)	Cpx (n = 40)
SiO <sub>2</sub>	41.2	39.3	37.4	54.8	57.6	-	49.8	53.0
TiO <sub>2</sub>	-	-	-	-	-	1.53	0.882	0.103
Al <sub>2</sub> O <sub>3</sub>	-	-	-	-	0.170	19.6	4.05	1.72
Cr <sub>2</sub> O <sub>3</sub>	-	-	-	-	-	32.8	-	0.425
FeO*	6.90	12.40	20.1	0.877	1.50	40.8	13.1	5.14
MnO	0.423	-	-	-	-	-	-	-
MgO	51.5	48.3	42.5	18.5	24.0	5.32	14.5	16.5
CaO	-	-	-	25.8	12.1	-	17.7	23.2
Total	100	100	100	100	95.3	100	100	100
Mg#				0.974	0.966	0.249	0.663	0.851
Fo value	93.0	87.4	79.0					
Cr#						0.530		

The data are displayed to three significant digits. FeO\* is total iron as FeO. t-1: type-1 olivine, t-2: type-2 olivine, and t-3: type-3 olivine.

Mg#:  $\text{Mg}/(\text{Mg} + \text{Fe})$  mol% in clinopyroxene, Tremolite, and Cr-spinel.

Fo value:  $100 \times \text{Mg}/(\text{Mg} + \text{Fe})$  mol% in olivine.

Cr#:  $\text{Cr}/(\text{Cr} + \text{Al})$  mol% in Cr-spinel.

### Chemical composition of the KUM Minerals

Samples were collected from localities 1 and 2 along the Kurotani Valley (Figs. 4 and 6). Two groups of olivine distinguished by their brightness in back-scatter electron imaging are further divided into three, type-1, type-2, and type-3, in terms of Fo value. Locality 1 yielded olivine of types 2 and 3, while locality 2 yields types 1 and 2. Type 1 olivine is  $\text{Fo}_{89-95}$ , type 2 is  $\text{Fo}_{81-92}$ , and type 3 is  $\text{Fo}_{78-85}$  (Fo value =  $100 \times \text{Mg}/(\text{Mg} + \text{Fe})$  mol%) (Fig. 10). SiO<sub>2</sub> concentration, 36–43 wt%, shows a positive correlation with Fo value (Fig. 10). Granular/columnar Cpx in the rock (3) exposed at the locality 2 varies from 0.93 to 0.98 (0.96 average) in Mg# (=  $\text{Mg}/(\text{Mg} + \text{Fe})$  mol%). CaO is 24–27 wt% (26 wt% average), and Al<sub>2</sub>O<sub>3</sub> is up to 0.32 wt% in Cpx. Tremolite is 0.92 to 0.98 (0.96 average) in Mg#. In Cr-spinel,  $\text{Mg}/(\text{Mg} + \text{Fe}^{2+})$  is 0.19–0.32 (0.23 average), and Cr# (=  $\text{Cr}/(\text{Cr} + \text{Al})$  mol%) is 0.47–0.56 (0.50 average). Al<sub>2</sub>O<sub>3</sub> is 15–23 wt% (21 wt% average), MgO is 3.9–6.9 wt% (4.9 wt% average), FeO\* is 36–49 wt% (41 wt% average), and Cr<sub>2</sub>O<sub>3</sub> is 27–34 wt% (31 wt% average) in Cr-spinel.

### Cpx chemical composition of basalts A and B of the Iwatsubodani Formation

Samples of basalt A were collected from locality 3, and of basalt B from locality 4 (Fig. 4). The Cpx chemistries

of basalts A and B are described below.

### (1) Basalt A

The Cpx varies from 0.41 to 0.79 in Mg# (0.65 average). TiO<sub>2</sub> is up to 1.47 wt.% (0.71 wt.% average), Al<sub>2</sub>O<sub>3</sub> ranges from 1.9 to 7.5 wt.% (3.4 wt.% average), and CaO is 12–21 wt.% (17 wt.% average). Cr<sub>2</sub>O<sub>3</sub> is less than 0.53 wt.%, and Na<sub>2</sub>O is less than 0.88 wt%.

### (2) Basalt B

The Mg# of Cpx (0.75–0.90, 0.81 average) in basalt B is generally higher than that of basalt A. TiO<sub>2</sub> is up to 0.51 wt.%, Al<sub>2</sub>O<sub>3</sub> varies from 1.3 to 3.7 wt.% (2.5 wt.% average), and CaO is 19–23 wt.% (21 wt.% average). Cr<sub>2</sub>O<sub>3</sub> is less than 0.89 wt.%, and Na<sub>2</sub>O is less than 0.32 wt%.

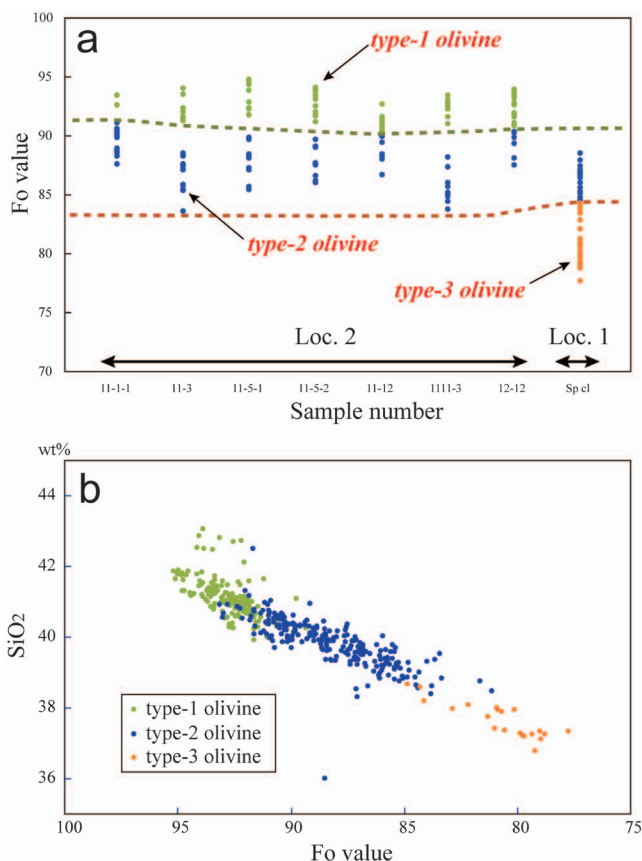


**Fig. 10** (a) Fo value ( $= 100 \times \text{Mg}/(\text{Mg} + \text{Fe}) \text{ mol}\%$ ) of the three types of olivine in selected samples. Loc.: locality. (b) SiO<sub>2</sub>–Fo value relationship of olivine.

## Discussion

### *What the three types of olivine in the KUM suggest?*

Olivine in the KUM is divided into three types, types-1, -2, and -3, in their Fo values. The type-1 is generally embedded in the type-2, and the type-2 is commonly enclosed within the type-3. This observation strongly suggests that the olivine was crystallized in order from the type-1 to type-3. It is generally known that the Fo value in earlier-crystallized olivine is higher than that of the later-crystallized one. The fact that the types-1 and -3 have highest and lowest Fo values respectively and the type-2 is medium between them gives a concrete evidence to above view. The locality 1 yields lower-Fo olivine (types-2 and -3) and the locality 2 is of higher-Fo olivine (types-1 and -2). The inference from this fact that the rock of the locality 1 was formed later than the locality 2, namely the locality 1 is an upper horizon than the locality 2 in a cumulate body.

### *Magmatic relationship between the KUM and the Iwatsubodani Formation*

This section discusses the magmatic relationship between the KUM and the mafic lava of the Iwatsubodani Formation (basalts A and B), based on their Cpx chemical composition. Two lines of evidence show that Cpx in the KUM was formed as a primary mineral before serpentinization and thermal metamorphism: (1) serpentine was produced along cleavages of Cpx, and (2) Cpx is cut by tremolite. The Cpx in the KUM (Mg# = 0.96 average) is assigned to diopside, and that in basalt A (Mg# = 0.65 average) and basalt B (Mg# = 0.81 average) is augite and diopside–augite (Fig. 11). The data from the KUM and the basalts of the Iwatsubodani Formation show a trend in

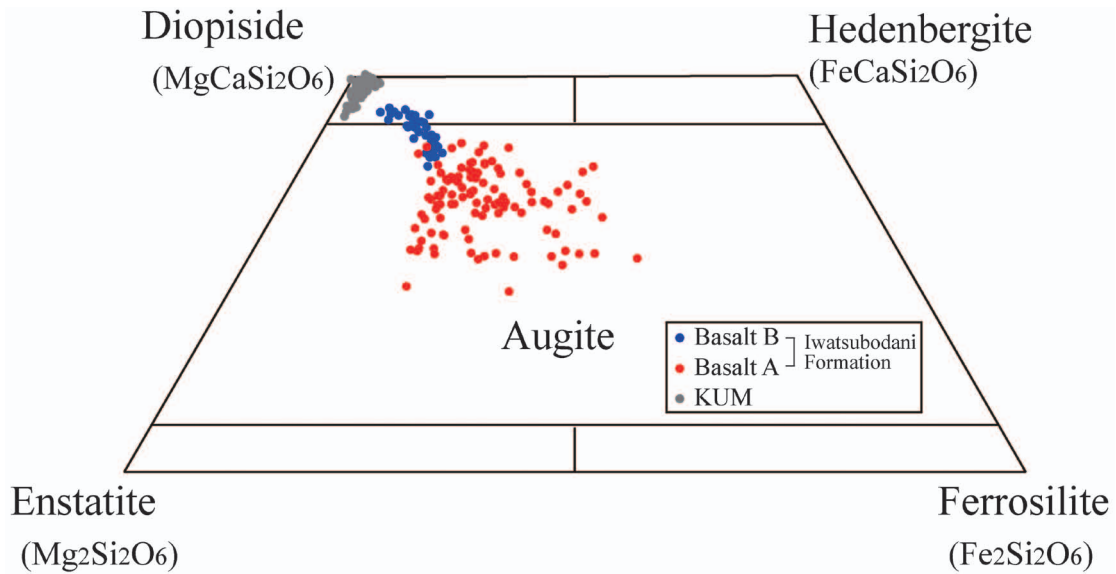


**Fig. 11** Data plot of the clinopyroxene chemical composition on the pyroxene trapezoid.

variation diagrams of Si, Al, Ti, Mg, Fe, and Ca (Fig. 12). Taken together, data from the KUM and the basalts of the Iwatsubodani Formation show a trend in both the pyroxene trapezoid and variation diagrams which is evidence that both these Cpx originated from a single magma source under a fractionation process. If this is correct, the KUM and the Iwatsubodani Formation likely form a pair of cumulate and eruptive rocks. The Iwatsubodani Formation is older than Silurian as mentioned before, and probably of Ordovician age (Tsukada, 1997; Tsukada et al., 2017). The chemical composition of the Iwatsubodani Formation clearly points to an arc volcanism (e.g., Tsukada et al., 2017). Taking all these lines of evidence together, the KUM–Iwatsubodani formation is probably the fossilized remains of an Ordovician(?) volcanic arc at the Eurasian continental margin.

Na and Cr data do not show any specific trends but are randomly scattered in the variation diagram (Fig. 12), probably because the samples do not contain enough of these elements to allow a reliable analysis. For instance, the  $\text{Na}_2\text{O}$  and  $\text{Cr}_2\text{O}_3$  concentrations of the basalts of the Iwatsubodani Formation are mostly less than 0.5 wt%, and the method used in this study is not applicable for elements present at less than 0.5 wt%.

*Why is Cpx Mg# higher in basalt B than basalt A?*

If the Cpx in both basalts A and B had crystallized from erupted melt, the former should have higher Mg# than the latter, since basalt B overlies basalt A (Tsukada, 1997; Tsukada et al., 2017). But in reality, the Mg# in basalt B is much higher than that of basalt A (Fig. 12). The data for basalts A and B were obtained from interstitial anhedral crystals and euhedral phenocrysts, respectively (Fig. 9c, d) implying that the Cpx in basalt A was rapidly crystallized from erupted melt while that in basalt B slowly crystallized in a magma chamber.

It is generally considered that when crystals grow rapidly a diffusion layer is formed around the crystals, and that this leads to variations in local melt concentration that produce a similarly variable crystal composition. However, when crystals grow slowly, the surrounding melt becomes homogeneous through concentration diffusion and convective stirring, and the composition of the crystals changes regularly by fractional crystallization in the magma. The Cpx data of basalt A are much more scattered than those of basalt B (Figs. 11 and 12) and this probably represents rapid crystallization of Cpx in basalt A from lack of homogeneity in the melt, while the linear

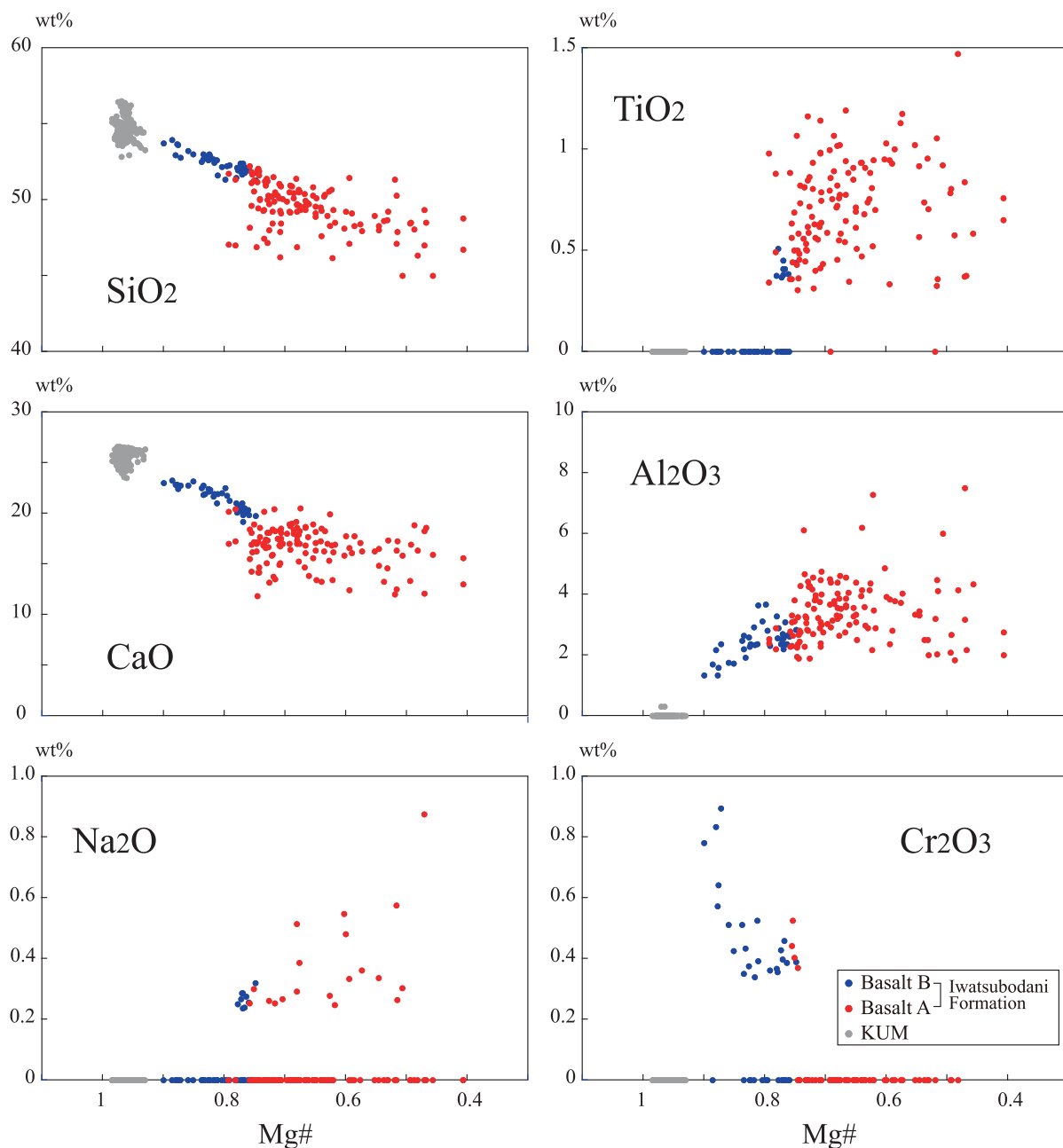


**Fig. 12** Variation diagrams for clinopyroxene from the Kurotani ultra-mafic rock (KUM) and the basalts A and B of the Iwatsubodani Formation.

data distribution of basalt B represents slow crystallization from a more homogenous melt in the magma chamber, through a process of fractional crystallization. This supports the results of the microscopic observation.

The deduction is that the Cpx in basalt A crystallized rapidly from erupted melt, while that in basalt B crystallized before its eruption in the magma chamber. In other words, the reason that the Cpx of basalt B is higher in Mg# than that of basalt A is that the former had already been crystallized in the magma chamber before the basalt A stage.

#### *Prospects for the tectonics of the HGB*

Tsukada et al. (2017) inferred that the Hitoegane-type of the Hida Gaien belt and the Oeyama ophiolite probably

shared an oceanic arc system at early Paleozoic supra-subduction zone. Given that this view is correct, it seems quite probable that the KUM is correlated to a part of the Oeyama ophiolite (Fig. 1). Although trace element (less than 0.5 wt%) compositions of olivine, pyroxene, Cr-spinel, and tremolite are essential to make a discussion in their correlation (e.g., Machi and Ishiwatari, 2010), the precision of the present data of trace elements is not sufficient to be examined in detail. Thus, this remains to be confirmed when accurate data of trace elements for the KUM's minerals become available.

Tsukada (2003) described the brittle and ductile shear zones in and around the HGB, and concluded that the geological outline of the HGB was completed through the Jurassic dextral and the Cretaceous sinistral movements along the eastern Eurasian continental margin. The Iwatsubodani Formation has been thrust over the KUM along a consolidated cataclastic shear zone at the Kurotani Valley, and an asymmetric structure in the shear zone shows top-to-the northwest sense of shearing. The fact that the cataclasite binding them together has a dextral strike-slip component suggests that the KUM and the Iwatsubodani Formation may have been juxtaposed by dextral movement during the Jurassic. Further chronological constraint of the movement on the shear zone is necessary for understanding of the tectonic developments of the HGB.

### Conclusion

1. Cpx data from the KUM and the basalts of the Iwatsubodani Formation together form a single trend in the variation diagram suggesting that they originated from a single magma source through fractionation.
2. The KUM and the Iwatsubodani Formation are likely a pair of cumulate and eruptive rocks formed at an Ordovician(?) volcanic arc in the Asian continental margin.
3. In the Iwatsubodani Formation, basalt A with interstitial anhedral Cpx, is overlain by basalt B with euhedral Cpx phenocrysts (Tsukada, 1997; Tsukada et al., 2017), and the former has lower Mg# than the latter. The Cpx of basalt B are therefore likely to have been crystalized in the magma chamber before the basalt A stage.

### Acknowledgements

This study includes the master's study of the first author at the University of Toyama, Japan. The first author is very grateful to Emeritus Profs. E. Horikoshi and O. Ujike and Prof. S. Otoh, for their helpful advice. He also appreciates the kind support during his field work from Mr. and Mrs. Karatani. In addition, all the authors thank Profs. M. Takeuchi and H. Yoshida of Nagoya University, and Prof. S. Kojima of Gifu University for their valuable comments. Dr. Giles Clarke at the Natural History Museum of London is thanked for his critical reading of the manuscript. Special thank goes to Dr. Y. Kouketsu at Nagoya University for reviewing this paper.

### References

- Adachi, S. (1985) Smaller foraminifers of the Ichinotani Formation (Carboniferous–Permian), Hida Massif, Central Japan. *Scientific Reports of the Institute of Geoscience, University of Tsukuba*, **B6**, 59–139.
- Ehiro, M., Tsujimori, T., Tsukada, K., and Nuramkhaan, M. (2016) Paleozoic basement and associated cover. Moreno, T., Wallis, S., Kojima, T., and Gibbons, W. (eds.), *The Geology of Japan*, 25–60. The Geological Society of London, London.
- Harayama, S. (1990) *Geology of the Kamikochi District. With Geological Sheet Map at 1: 50,000*, Geological Survey of Japan, Tsukuba, 175 p.
- Horikoshi, E., Tazawa, J., Naito, N., and Kaneda, J. (1987) Permian brachiopods from Moribu, north of Takayama City, Hida Mountains, central Japan. *Journal of the Geological Society of Japan*, **93**, 141–143.

- Igo, H. (1956) On the Carboniferous and Permian of the Fukuji district, Hida Massif, with special reference to the fusulinid zones of the Ichinotani Group. *Journal of the Geological Society of Japan*, **62**, 217–240.
- Igo, H. (1990) Paleozoic strata in the Hida “Gaien” Belt. Ichikawa, K., Mizutani, S., Hara, I., Hada, S. and Yao, A. (eds.), *Pre-Cretaceous Terranes of Japan*, 41–48. IGCP Project No 224: Pre-Jurassic Evolution of Eastern Asia, Osaka.
- Kamei, T. (1955) Hida Gaien tectonic zone. *Hida-sanchi no Chishitsu Kenkyu Renrakushi*, **7**, 10–12.
- Kunugiza, K. and Maruyama, S. (2011) Geotectonic Evolution of the Hida Marginal Belt, Central Japan: Reconstruction of the oldest Pacific-type orogeny of Japan. *Journal of Geography*, **120**, 960–980.
- Kuroda, Y. and Shimoda, S. (1967), Olivine with well-developed cleavages its geological and mineralogical Meanings. *Journal of the Geological Society of Japan*, **73**, 377–388.
- Machi, S. and Ishiwatari, A. (2010) Ultramafic rocks in the Kotaki area, Hida Marginal Belt, central Japan: peridotites of the Oeyama ophiolite and their metamorphism. *Journal of the Geological Society of Japan*, **116**, 293–308.
- Manchuk, N., Kurihara, T., Tsukada, K., Kochi, Y., Obara, H., Fujimoto, T., Orihashi, Y., and Yamamoto, K. (2013) U-Pb zircon age from the radiolarian-bearing Hitoegane Formation in the Hida Gaien Belt, Japan. *Island Arc*, **22**, 494–507.
- Niikawa, I. (1980) Geology and biostratigraphy of the Fukuji district, Gifu Prefecture, Central Japan. *Journal of the Geological Society of Japan*, **86**, 25–36.
- Niwa, M., Hotta, K., and Tsukada, K. (2004) Middle Permian fusulinoideans from the Moribu Formation in the Hida-gaien Tectonic Zone, Nyukawa Village, Gifu Prefecture, central Japan. *Journal of the Geological Society of Japan*, **110**, 384–387.
- Taira, A., Ohara, Y., Wallis, S., Ishiwatari, A., and Iryu, Y. (2016) Geological evolution of Japan: an overview. Moreno, T., Wallis, S., Kojima, T., and Gibbons, W. (eds.), *The Geology of Japan*, 1–24. The Geological Society of London, London.
- Takeuchi, M., Kawai, M., Noda, A., Sugimoto, N., Yokota, H., Kojima, S., Ohno, K., Niwa, M., and Ohba, H. (2004) Stratigraphy of the Permian Shiroumadake Formation and its structural relationship with serpentinite in the Mt. Shiroumadake area, Hida Gaien belt, central Japan. *Journal of the Geological Society of Japan*, **110**, 715–730.
- Tazawa, J., Hasegawa, Y., and Yoshida, K. (2000a) Schwagerina (Fusulinacean) and Choristites (Brachiopoda) from the Carboniferous Arakigawa Formation in the Hidagaien Belt, central Japan. *Earth Sciences (Chikyu-Kagaku)*, **54**, 196–199.
- Tazawa, J., Yang, W., and Miyake, Y. (2000b) Cyrtospirifer and Leptophloeum from the Devonian Rosse Formation, Hida Gaien Belt, central Japan. *Journal of the Geological Society of Japan*, **106**, 727–735.
- Tazawa, J., Tsushima, K., and Hasegawa, Y. (1993) Discovery of Monodioxodina from the Permian Moribu Formation in the Hida Gaien Belt, Central Japan. *Earth Sciences (Chikyu-Kagaku)*, **4**, 345–348.
- Tazawa, J., Niikawa, I., Furuichi, K., Miyake, Y., Ohkura, M., Furutani, H., and Kaneko, N. (1997) Discovery of Devonian tabulate corals and crinoids from the Moribu district, Hida Gaien Belt, central Japan. *Journal of the Geological Society of Japan*, **103**, 399–401.
- Tsukada, K. (1997) Stratigraphy and structure of Paleozoic rocks in the Hitoegane area, Kamitakara Village, Gifu Prefecture. *Journal of the Geological Society of Japan*, **103**, 658–668.
- Tsukada, K. (2003) Jurassic Dextral and Cretaceous Sinistral Movements Along the Hida Marginal Belt. *Gondwana Research*, **6**, 687–698.
- Tsukada, K. (2018) Quantitative analysis of chemical composition of anhydrous silicate minerals using SEM-EDX installed at Nagoya University Museum. *Bulletin of the Nagoya University Museum*, **34**, 1–10.
- Tsukada, K. (2021) Quantitative analysis of chemical composition of hydrous silicate minerals using SEM-EDX installed at Nagoya University Museum. *Bulletin of the Nagoya University Museum*, **36**, 1–9.
- Tsukada, K. and Niwa, K. (2005) The Triassic Tandodani Formation in the Hongo area, Hida Gaien belt, central Japan. *Journal of Earth and Planetary Science, Nagoya University*, **52**, 1–10.
- Tsukada, K. and Takahashi, Y. (2000) Redefinition of the Permian strata in the Hida-gaien Tectonic Zone, Fukuji area, Gifu Prefecture, Central Japan. *Journal of Earth and Planetary Science, Nagoya University*, **31**, 1–35.

- Tsukada, K., Takahashi, Y., and Ozawa, T. (1999) Stratigraphic relationship between the Mizuyagadani and Sorayama Formations, and age of the Sorayama Formation, in the Hida-gaien Tectonic Zone, Kamitakara Village, Gifu Prefecture, central Japan. *Journal of Geological Society of Japan*, **105**, 496–507.
- Tsukada, K., Takeuchi, M., and Kojima, S. (2004) Redefinition of the Hida Gaien belt. *Journal of Geological Society of Japan*, **110**, 640–658.
- Tsukada, K., Yamamoto, K., Gantumur, O., and Nuramkhaan, M. (2017) Early Paleozoic subduction initiation volcanism of the Iwatsubodani Formation, Hida Gaien belt, Southwest Japan. *International Journal of Earth Sciences*, **106**, 1429–1451.